HOKKAIDO UNIVERSITY

Title	Giant tunneling magnetoresistance in epitaxial Co2MnSi/MgO/Co2MnSi magnetic tunnel junctions by half-metallicity of Co2MnSi and coherent tunneling
Author(s)	Liu, Hong-xi; Honda, Yusuke; Taira, Tomoyuki; Matsuda, Ken-ichi; Arita, Masashi; Uemura, Tetsuya; Yamamoto, Masafumi
Citation	Applied Physics Letters, 101(13), 132418 https://doi.org/10.1063/1.4755773
Issue Date	2012-09-24
Doc URL	http://hdl.handle.net/2115/50424
Rights	Copyright 2012 American Institute of Physics. This article may be downloaded for personal use only. Any other use requires prior permission of the author and the American Institute of Physics. The following article appeared in Appl. Phys. Lett. 101, 132418 (2012) and may be found at https://dx.doi.org/10.1063/1.4755773
Type	article
File Information	APL101-13_132418.pdf

Giant tunneling magnetoresistance in epitaxial Co2MnSi/MgO/Co2MnSi magnetic tunnel junctions by half-metallicity of Co2MnSi and coherent tunneling

Hong-xi Liu, Yusuke Honda, Tomoyuki Taira, Ken-ichi Matsuda, Masashi Arita et al.

Related Articles

Angular-dependences of giant in-plane and interlayer magnetoresistances in Bi2Te3 bulk single crystals
Appl. Phys. Lett. 101, 152107 (2012)

Magnetic field-dependent effective microwave properties of microwire-epoxy composites
Appl. Phys. Lett. 101, 152905 (2012)

Giant magnetoresistance effect in graphene with asymmetrical magnetic superlattices
Appl. Phys. Lett. 101, 152404 (2012)

Giant magneto-resistance estimated from direct observation of nanoscale ferromagnetic domain evolution in La0.325Pr0.3Ca0.375MnO3
J. Appl. Phys. 112, 053924 (2012)

Electrical determination of relative chirality direction in a Co/Cu/Co ferromagnetic ring
Appl. Phys. Lett. 101, 062409 (2012)

Additional information on Appl. Phys. Lett.

Journal Homepage: http://apl.aip.org/

Journal Information: http://apl.aip.org/about/about_the_journal

Top downloads: http://apl.aip.org/features/most_downloaded

Information for Authors: http://apl.aip.org/authors

Giant tunneling magnetoresistance in epitaxial Co₂MnSi/MgO/Co₂MnSi magnetic tunnel junctions by half-metallicity of Co₂MnSi and coherent tunneling

Hong-xi Liu, Yusuke Honda, Tomoyuki Taira, Ken-ichi Matsuda, Masashi Arita, Tetsuya Uemura, and Masafumi Yamamoto[a)]
Division of Electronics for Informatics, Graduate School of Information Science and Technology, Hokkaido University, Sapporo 060-0814, Japan

Giant tunnel magnetoresistance (TMR) ratios of up to 1995% at 4.2 K and up to 354% at 290 K were obtained for epitaxial Co₂MnSi/MgO/Co₂MnSi magnetic tunnel junctions (MTJs) featuring a reduced lattice mismatch in the MTJ trilayer by introducing a thin Co₂MnSi lower electrode deposited on a Co₅₀Fe₅₀ buffer layer. The obtained giant TMR ratios can be explained by the enhanced contribution of coherent tunneling originating from the increased misfit dislocation spacing at the lower and upper interfaces with a MgO barrier along with the half-metallicity of Co₂MnSi electrodes. © *2012 American Institute of Physics*. [http://dx.doi.org/10.1063/1.4755773]

Spintronic devices, which manipulate the spin degree of freedom in addition to the charge of the electron, have attracted much interest as promising future electron devices because they are expected to provide nonvolatility, reconfigurable logic functions, and ultralow power consumption.[1,2] For spintronic devices, the creation of a highly spin-polarized current is essential. One of the most suitable types of spin source materials for spintronic devices is half-metallic ferromagnets[3] because of their complete spin polarization at the Fermi level (E_F). Co-based Heusler alloys (Co_2YZ, where Y is usually a transition metal and Z is a main group element) have attracted much interest as highly spin-polarized materials.[4–14] This is because of the half-metallic nature theoretically predicted for many of these alloys[15–17] and because of their high Curie temperatures, which are well above room temperature (RT).[18] Co_2YZ thin films have been widely applied to magnetic tunnel junctions (MTJs), in particular, in combination with a MgO barrier.[7–10]

In epitaxial single-crystalline magnetic tunnel junctions, coherent tunneling—in which the transversal crystal momentum of a tunneling electron is conserved—results in a tunneling probability that depends on the symmetry of the wave functions of the tunneling electrons.[19,20] The importance of enhanced tunneling probability for electrons in specific Bloch states (Δ_1 states in for example, Fe, $Co_{1−x}Fe_x$, and CoFeB) in epitaxial MgO-based MTJs due to coherent tunneling has been revealed theoretically and experimentally.[19–24] Indeed, due to the coherent tunneling effect, tunnel magnetoresistance (TMR) ratios of up to 1144% at 5 K and up to 604% at 300 K have been demonstrated for CoFeB/MgO/CoFeB MTJs.[24]

Co₂MnSi is one of the most extensively studied Heusler alloys[5–7,12–14] because of its theoretically predicted half metallic nature[15–17] and because of its high Curie temperature of 985 K.[18] Epitaxial heterostructures consisting of Co₂MnSi, which has Δ_1 states at E_F for the majority-spin band, and a MgO barrier are advantageous as spin sources for spintronic devices. This is because Co₂MnSi/MgO heterostructures fea-

ture both intrinsically high spin polarization arising from the half-metallic nature of Co₂MnSi and enhanced tunneling spin polarization due to coherent tunneling of electrons having Δ_1 states for the majority-spin band.[25]

We have recently investigated the effect of defects in Co₂MnSi thin films on spin-dependent tunneling characteristics.[26,27] We obtained higher TMR ratios for Co₂MnSi/MgO/Co₂MnSi MTJs with Mn-rich Co₂MnSi electrodes and we observed high TMR ratios of 1135% at 4.2 K and 236% at RT.[26] The observed higher TMR ratios for MTJs with Mn-rich Co₂MnSi electrodes suggested that detrimental Co_{Mn} antisites[13] can be suppressed by preparing Co₂MnSi films with a Mn-rich composition.[26,27]

On the other hand, epitaxial interfaces between the electrodes and the MgO barrier are essential for coherent tunneling for which the electron momentum parallel to the plane is conserved: coherent tunneling does not occur for a region of the interface where a misfit dislocation exists. Yuasa *et al*. noted that a reduced misfit dislocation density at the MgO barrier/upper Fe layer interface in epitaxial Fe/MgO/Fe MTJs resulted in an increased TMR ratio.[21] Bonell *et al*. investigated how the TMR ratio of epitaxial Fe/MgO/Fe MTJs depended on the misfit dislocation density at the interface by replacing the Fe lower electrode by Fe-V alloy films and showed that the TMR ratio was enhanced by better structural coherency.[28]

Our purpose in the present study was to clarify the contributions from coherent tunneling and the half-metallicity of Co₂MnSi thin films to the TMR characteristics in fully epitaxial MTJs with Co₂MnSi films as both lower and upper electrodes and a MgO barrier. To do this, we investigated how improved interfacial structural properties affect the TMR characteristics of Co₂MnSi/MgO/Co₂MnSi MTJs (Co₂MnSi MTJs). In our previous studies of Co₂MnSi-based MTJs, we used a thick (typically 30-nm) Co₂MnSi lower electrode grown on MgO-buffered MgO(001) substrates.[7,26] This thick Co₂MnSi layer was relaxed on the MgO-buffered MgO(001) substrate, causing a relatively large lattice mismatch of −5.1% between the fully relaxed Co₂MnSi layer and the MgO barrier with a 45° in-plane rotation. To improve the interfacial structural properties, we considered

[a)]Author to whom correspondence should be addressed. Electronic mail: yamamoto@nano.ist.hokudai.ac.jp.

the facts that the lattice mismatch between Co_2MnSi and $Co_{50}Fe_{50}$ (CoFe) is very small (−0.8%) and that the lattice mismatch of −4.3% between CoFe and MgO with a 45° in-plane rotation is smaller than −5.1%, which is the lattice mismatch between a fully relaxed Co_2MnSi lower electrode and MgO. On the basis of these considerations, we introduced a thin (typically 3-nm) Co_2MnSi lower electrode grown on a CoFe-buffered MgO(001) substrate instead of the previously used thick Co_2MnSi lower electrode grown on a MgO-buffered MgO(001) substrate.

The fabricated MTJ layer structures were as follows: (from the substrate side) MgO buffer (10 nm)/CoFe buffer (30 nm)/Co_2MnSi lower electrode (3 nm)/MgO barrier (1.4–3.2 nm)/Co_2MnSi upper electrode (3 nm)/layers for exchange biasing/Ru cap (5 nm), grown on MgO(001) single-crystal substrates. Compared with our previous work,[26] we introduced a CoFe buffer instead of depositing the MTJ trilayer onto the MgO buffer and we also reduced the Co_2MnSi lower electrode thickness from 30 to 3 nm. To fully investigate structural properties and spin-dependent tunneling characteristics, we prepared three series of CoFe-buffered Co_2MnSi MTJs having $Co_2Mn_\alpha Si_\gamma$ electrodes with slightly different Si compositions γ with respect to Co_2: these were $Co_2Mn_{1.29}Si_{1.0}$ (MTJ-A), $Co_2Mn_{1.35}Si_{0.88}$ (MTJ-B), and $Co_2Mn_\alpha Si_{0.96}$ (MTJs of series C with various values of α). The layer structures for exchange biasing for these MTJ series were (above the Co_2MnSi upper electrode) Ru (0.8 nm)/$Co_{90}Fe_{10}$ (2 nm)/$Ir_{22}Mn_{78}$ (10 nm) for MTJ-A and $Co_{50}Fe_{50}$ (1.1 nm)/$Ir_{22}Mn_{78}$ (10 nm) for MTJ-B and MTJs of series C. (The slightly different layer structures for exchange biasing were not critical for TMR characteristics.)

The fabrication procedure for these MTJ layer structures was the same as for MgO-buffered Co_2MnSi MTJs,[26] except for the abovementioned changes. Briefly, we prepared Co_2MnSi electrodes by co-sputtering from a nearly stoichiometric Co_2MnSi target and a Mn target.[26] The CoFe buffer, Co_2MnSi lower electrode, MgO barrier, Co_2MnSi upper electrode, IrMn layer were all deposited at RT. The MTJ layer structure was annealed *in situ* at 500 °C just after deposition of the CoFe buffer and at 550 °C both just after deposition of the Co_2MnSi lower electrode and fairly soon after deposition of the Co_2MnSi upper electrode. We fabricated MTJs with these layer structures by photolithography and Ar ion milling. The fabricated junction size was $10 \times 10 \mu m^2$. After the microfabrication, MTJs were annealed *ex situ* at 350 °C in a vacuum of 5×10^{-2} Pa under a magnetic field of 5 kOe to enable exchange biasing on the upper Co_2MnSi electrode. We defined the TMR ratio as $(R_{AP}–R_P)/R_P$, where R_{AP} and R_P are the resistances for the antiparallel and parallel magnetization configurations between the upper and lower electrodes.

We now describe the structural properties of the prepared Co_2MnSi MTJ layer structures. For structural characterization, cross-sectional HRTEM lattice images and two-beam bright-field TEM images of an as-prepared Co_2MnSi MTJ layer structure having a Mn-rich film composition of $Co_2Mn_{1.29}Si$ (MTJ-A) were obtained.

Figure 1(a) shows a cross-sectional HRTEM lattice image of an as-prepared CoFe-buffered Co_2MnSi MTJ layer structure consisting of (from the lower side) CoFe buffer/lower Co_2MnSi (3 nm)/MgO barrier (~2.5 nm)/upper

Co_2MnSi (3 nm)/Ru (0.8 nm)/$Co_{90}Fe_{10}$ (2 nm)/$Ir_{22}Mn_{78}$ (10 nm)/Ru cap (5 nm) with Mn-rich $Co_2Mn_{1.29}Si$ electrodes (MTJ-A); it was taken along the [1-10] direction of the Co_2MnSi layers. This image clearly shows that all these layers were grown epitaxially and were single-crystalline. It was also confirmed that atomically flat and abrupt interfaces were formed. Importantly, there were no lattice misfit dislocations between the CoFe buffer and the Co_2MnSi lower electrode. This indicates that the Co_2MnSi lower electrode was lattice-matched to the CoFe buffer. Figures 1(b) and 1(c) show nano-beam electron diffraction patterns (beam diameter: 2 nm) for the Co_2MnSi lower and upper electrodes, where 111 spots specific to the $L2_1$ structure were observed in addition to 002 spots specific to the B2 and $L2_1$ structures, indicating that both the Mn-rich $Co_2Mn_{1.29}Si$ lower and upper electrodes had the $L2_1$ structure.

Simultaneously with the HRTEM and electron diffraction observations, energy dispersive x-ray spectroscopy (EDS) line analysis (beam diameter: 0.7 nm) was performed for the same sample as in Fig. 1. This analysis indicated no appreciable diffusion of Mn from the Co_2MnSi lower and upper electrodes to the Co_2MnSi electrode/MgO barrier interfaces or into the MgO barrier. (Note that the IrMn layer had not yet been deposited when the MTJ layer structure was *in-situ* annealed twice at 550 °C.) It also indicated that the diffusion of Fe from the CoFe buffer layer into the Co_2MnSi lower electrode was not appreciable.

To further characterize the interfacial structural quality of CoFe-buffered Co_2MnSi MTJs, we investigated misfit
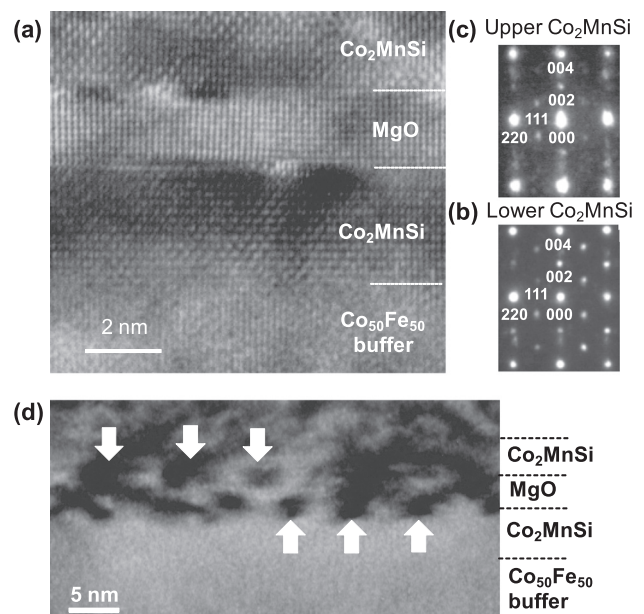

FIG. 1. (a) Cross-sectional HRTEM lattice image of a CoFe-buffered Co_2MnSi MTJ layer structure consisting of (from the lower side) $Co_{50}Fe_{50}$ (CoFe) buffer/lower Co_2MnSi (3 nm)/MgO barrier (~2.5 nm)/upper Co_2MnSi (3 nm)/Ru (0.8 nm)/$Co_{90}Fe_{10}$ (2 nm)/$Ir_{22}Mn_{78}$ (10 nm)/Ru cap (5 nm) with Mn-rich $Co_2Mn_{1.29}Si$ electrodes (MTJ-A); it was taken along the [1-10] direction of the Co_2MnSi. (b) and (c) Nano-beam electron diffraction patterns for the lower (b) and upper (c) Co_2MnSi electrodes; the beam diameter was 2 nm. (d) Two-beam bright-field TEM image of a CoFe-buffered Co_2MnSi MTJ layer structure with Mn-rich $Co_2Mn_{1.29}Si$ electrodes (the same sample as shown in Figs. 1(a)–1(c)) excited with reciprocal vectors parallel to the plane ($g = [200]_{MgO}$ and $[220]_{Co2MnSi}$). The arrows provide a guide to show the misfit dislocation contrasts.

dislocation densities at the interfaces with the MgO barrier through two-beam bright-field TEM images. Figure 1(d) shows a two-beam bright-field TEM image of a CoFe-buffered Co_2MnSi MTJ layer structure with Mn-rich $Co_2Mn_{1.29}Si$ electrodes (the same sample shown in Figs. 1(a)–1(c)) excited with reciprocal vectors parallel to the plane ($g = [200]_{MgO}$ and $[220]_{Co2MnSi}$). The image shows the strain contrasts that arose from the periodically spaced misfit dislocations at the lower and upper interfaces with the MgO barrier. It also shows that the spacing of the misfit dislocations is almost constant. The dislocation spacing values at the lower and upper interfaces were 6.4 (1.0) and 6.2 (1.4) nm for the lower and upper interfaces, respectively, where the values in parentheses are the standard deviations. These values of the misfit dislocation spacing at the lower and upper interfaces of the CoFe-buffered Co_2MnSi MTJ were significantly larger than the value of 4.3 ± 0.1 nm observed for the lower and upper interfaces in an identically fabricated MgO-buffered Co_2MnSi MTJ.[29] Thus, the structural properties in both the lower and upper interfacial regions between the electrodes and the MgO barrier were improved in CoFe-buffered Co_2MnSi MTJs in the sense of the increased misfit dislocation spacing compared with MgO-buffered Co_2MnSi MTJs. This improvement can be explained as follows: the introduction of the CoFe buffer (which has a smaller lattice mismatch of -4.3% with MgO) and the thin (3-nm-thick) Co_2MnSi lower electrode resulted in the Co_2MnSi lower electrode lattice-matched to the CoFe buffer, leading to a reduction in the lattice mismatch in the MTJ trilayer.

We now describe the TMR characteristics of fabricated Co_2MnSi MTJs grown on CoFe-buffered MgO(001) substrates. Typical TMR curves at 4.2 K and 290 K for a fabricated fully epitaxial Co_2MnSi MTJ having Mn-rich $Co_2Mn_{1.35}Si_{0.88}$ elec-

TABLE I. Typical TMR ratios at 4.2 K and 290 K for a MTJ from each MTJ series MTJ-A to MTJ-C, which had slightly different Si compositions γ with respect to Co_2 in $Co_2Mn_\alpha Si_\gamma$ electrodes, and the respective film compositions of $Co_2Mn_\alpha Si_\gamma$ electrodes for each MTJ.

MTJ series	Film composition of a MTJ from each MTJ series	Typical TMR ratios	
		at 4.2 K	at 290 K
MTJ-A	$Co_2Mn_{1.29}Si_{1.0}$	1804%	344%
MTJ-B	$Co_2Mn_{1.35}Si_{0.88}$	1995%	330%
MTJ-C	$Co_2Mn_{1.37}Si_{0.96}$	1910%	354%

trodes (MTJ-B) are shown in Fig. 2. The MTJ exhibited clear exchange-biased TMR characteristics with giant TMR ratios of 1995% at 4.2 K and 330% at 290 K. These values are significantly higher than the 1135% at 4.2 K and 236% at 290 K previously obtained for Co_2MnSi MTJs grown on MgO-buffered MgO(001) substrates.[26] We confirmed these considerably enhanced TMR ratios by introducing a thin Co_2MnSi lower electrode deposited on a CoFe buffer layer for the three different series of CoFe-buffered Co_2MnSi MTJs. As summarized in Table I, all three series of the CoFe-buffered Co_2MnSi MTJs showed almost identical giant TMR ratios of up to 1995% at 4.2 K and up to 354% at 290 K.

We investigated how the TMR ratios of CoFe-buffered Co_2MnSi MTJs depended on the Mn composition in Co_2MnSi electrodes in MTJs of series C, which had $Co_2Mn_\alpha Si_{0.96}$ electrodes with various values of α. Figures 3(a) and 3(b) show the TMR ratios at 4.2 K and 290 K, respectively, for CoFe-buffered Co_2MnSi MTJs of series C as a function of Mn composition α ranging from 0.72 (Mn-deficient Co_2MnSi) to 1.57 (Mn-rich Co_2MnSi) in $Co_2Mn_\alpha Si_{0.96}$ electrodes, in comparison with those of MgO-buffered Co_2MnSi MTJs as a function of Mn composition α ranging from 0.69 (Mn-deficient Co_2MnSi) to 1.43 (Mn-rich Co_2MnSi) in $Co_2Mn_\alpha Si$ electrodes previously reported in Ref. 26. The TMR ratios at both 4.2 K
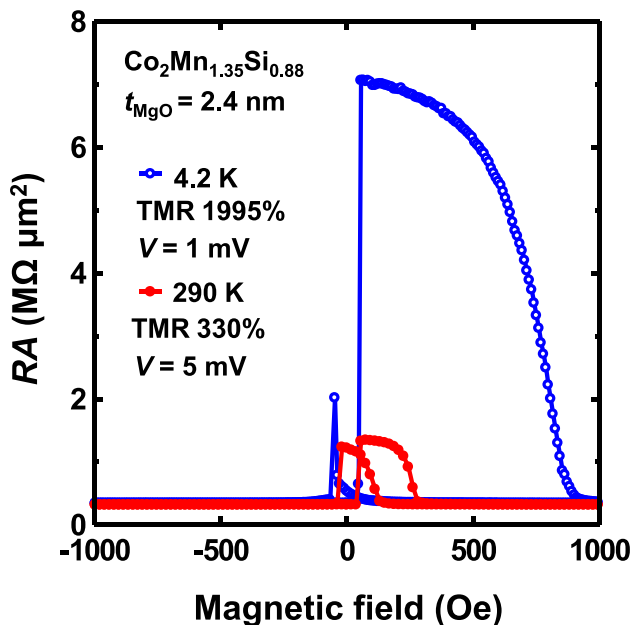
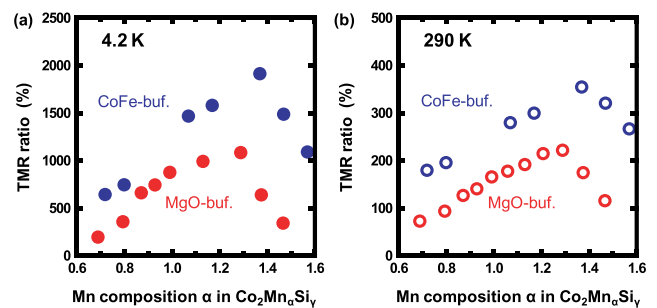FIG. 2. Typical TMR curves at 4.2 K and 290 K for a Co_2MnSi MTJ consisting of (from the lower side) Co_2MnSi lower electrode (3 nm)/MgO barrier (2.4 nm)/Co_2MnSi upper electrode (3 nm) grown on a CoFe-buffered MgO(001) substrate with Mn-rich $Co_2Mn_{1.35}Si_{0.88}$ electrodes (MTJ-B). The magnetoresistance was measured with a magnetic field applied along the [1-10] axis of the Co_2MnSi film using a dc four-probe method. The bias voltages were 1 mV at 4.2 K and 5 mV at 290 K.

FIG. 3. TMR ratios at (a) 4.2 K and (b) 290 K for fully epitaxial CoFe-buffered $Co_2Mn_\alpha Si_{0.96}$ (3 nm)/MgO/$Co_2Mn_\alpha Si_{0.96}$ (3 nm) MTJs of series C (blue solid and open circles are for 4.2 K and 290 K, respectively) as a function of Mn composition α ranging from 0.72 (Mn-deficient Co_2MnSi) to 1.57 (Mn-rich Co_2MnSi). The MgO tunnel barrier layer was deposited by electron beam evaporation using a linearly moving shutter with the nominal thickness (t_{MgO}) ranging from 1.4 to 3.2 nm on each 20×20 mm^2 substrate. The TMR ratio showed a slight increase with an increase in t_{MgO} for a t_{MgO} range from 1.8 to 3.0 nm. A typical TMR ratio in this t_{MgO} range for each Mn composition is plotted. For comparison, those of MgO-buffered $Co_2Mn_\alpha Si$ (30 nm)/MgO/$Co_2Mn_\alpha Si$ (3 nm) MTJs (red solid and open circles are for 4.2 K and 290 K, respectively) as a function of Mn composition α ranging from 0.69 (Mn-deficient Co_2MnSi) to 1.43 (Mn-rich Co_2MnSi) reported in Ref. 26 are plotted. The bias voltage was 1 mV at 4.2 K and 5 mV at 290 K. The Si compositions γ in the expression of $Co_2Mn_\alpha Si_\gamma$ are 0.96 for CoFe-buffered Co_2MnSi MTJs of series C and 1.0 for MgO-buffered Co_2MnSi MTJs.

and 290 K were found to increase systematically with increasing α for the range from $\alpha = 0.72$ to 1.37. Indeed, the TMR ratio at 4.2 K increased significantly from 640% for Mn-deficient $\alpha = 0.72$ to 1910% for Mn-rich $\alpha = 1.37$. The TMR ratio at 290 K also notably increased with increasing α: from 179% for $\alpha = 0.72$ to 354% for $\alpha = 1.37$. Thus, we obtained higher TMR ratios of 1910% at 4.2 K and 354% at 290 K for MTJs with Mn-rich $Co_2Mn_{1.37}Si_{0.96}$ electrodes than for those having Mn-deficient or almost stoichiometric Co_2MnSi electrodes in MTJs of series C. This confirms our previous observations[26,27,30] and can be explained by the higher half-metallicity enhanced through suppression of harmful Co_{Mn} antisites by using Mn-rich Co_2MnSi electrodes. We have proposed a site-specific formula unit composition model for Mn-rich $Co_2Mn_\alpha Si$ ($\alpha > 1$) that is based on the $L2_1$ structure, as confirmed by the structural analysis, and on the assumption of antisite formation rather than vacancy formation,[26,27] where this assumption was introduced by taking into account that the theoretically calculated formation energies for vacant sites are higher than those for antisites for Co_2MnSi.[13,14] According to this model, the nominal composition of $Co_2Mn_{1.37}Si_{0.96}$ (used in MTJs of series C) have the site-specific formula unit composition of $[Co_{1.85}Mn_{0.15}]Mn[Si_{0.89}Mn_{0.11}]$, in which Co_{Mn} antisites detrimental to the half-metallicity are suppressed.

Importantly, CoFe-buffered Co_2MnSi MTJs showed markedly higher TMR ratios at 4.2 K and 290 K than the previously reported TMR ratios of MgO-buffered Co_2MnSi MTJs for a wide α range from $\alpha = 0.72$ to 1.57, as shown in Figs. 3(a) and 3(b). To discuss a possible origin of the significantly enhanced TMR ratios of up to 1995% at 4.2 K and up to 354% at 290 K for CoFe-buffered Co_2MnSi MTJs with Mn-rich Co_2MnSi electrodes from the 1135% at 4.2 K and 236% at 290 K previously reported for MgO-buffered Co_2MnSi MTJs with Mn-rich Co_2MnSi electrodes,[26] we plotted how the TMR ratios at 4.2 K and 290 K of these two kinds of MTJ depended on the average misfit dislocation spacing at the interfaces with a MgO barrier in Figs. 4(a) and 4(b), where we classified the CoFe-buffered and MgO-buffered Co_2MnSi MTJs into group 1; these group-1 MTJs are characterized as

having Co_2MnSi thin films as both the lower and upper electrodes. As shown in Fig. 4, the CoFe-buffered Co_2MnSi MTJs that had the larger average misfit dislocation spacing than the MgO-buffered Co_2MnSi MTJs showed significantly higher TMR ratios at both 4.2 K and 290 K. This can be ascribed to the enhanced coherent tunneling contribution in the CoFe-buffered Co_2MnSi MTJs arising from the increased area of epitaxial interfaces without a misfit dislocation because epitaxial interfaces are essential for conservation of the electron transverse momentum for tunneling.

As recently reported elsewhere,[30] similar dependences of the TMR ratios at both 4.2 K and 290 K on the misfit dislocation spacing were also clearly observed for Co_2MnSi/MgO-based MTJs that had a Co_2MnSi film as either the lower or the upper electrode and a CoFe film as the other electrode (classified into group 2), including (from the lower side) (1) MgO buffer/Co_2MnSi/MgO/CoFe MTJs, (2) CoFe buffer/thin Co_2MnSi/MgO/CoFe MTJs, and (3) CoFe/MgO/Co_2MnSi MTJs, all having Mn-rich Co_2MnSi electrodes. Thus, it was commonly observed that the larger misfit dislocation spacing at the interfaces with a MgO barrier resulted in the larger TMR ratios at both 4.2 K and 290 K for both Co_2MnSi/MgO/Co_2MnSi MTJs (group 1) and MgO-based MTJs having a Co_2MnSi electrode and a CoFe electrode (group 2).

At low temperatures where thermally excited magnons can be ignored, the tunneling spin polarization and coherent tunneling contribution are the key factors that determine the TMR ratios of epitaxial MTJs. For comparison, we also plotted in Fig. 4(a) how the TMR ratio at 4.2 K depended on the average misfit dislocation spacing at the interfaces for the MTJs with a Co_2MnSi electrode and a CoFe electrode (group 2) from Ref. 30. It can be clearly seen from the comparison in Fig. 4(a) that MTJs having Co_2MnSi as both the lower and upper electrodes (group 1) showed significantly higher TMR ratios at 4.2 K of up to 1995% than the 1049% of MTJs having a Co_2MnSi electrode and a CoFe electrode (group 2).[30] This clearly demonstrates the significantly higher tunneling spin polarization of Co_2MnSi than CoFe and the half-metallic nature of Co_2MnSi as the origin of its high tunneling spin polarization. Furthermore, the much higher TMR ratios of up to 1995% at 4.2 K obtained for Co_2MnSi MTJs than the 1144% at 5 K reported for CoFeB/MgO/CoFeB MTJs[24] also definitely indicate the high spin polarization at E_F of Co_2MnSi electrodes as arising from the half-metallicity of Co_2MnSi because the high TMR ratio observed for the CoFeB/MgO/CoFeB MTJs is due solely to the coherent tunneling contribution of Δ_1 band electrons.

In summary, we demonstrated giant TMR ratios of up to 1995% at 4.2 K and up to 354% at 290 K for fully epitaxial Co_2MnSi/MgO/Co_2MnSi MTJs (Co_2MnSi MTJs) having Mn-rich Co_2MnSi electrodes. From the systematic study of the dependence of the TMR ratio of Co_2MnSi MTJs on the Mn composition in Co_2MnSi electrodes and on the misfit dislocation spacing at the interfaces with a MgO barrier, we conclude that the obtained giant TMR ratios can be ascribed to the half-metallicity of Co_2MnSi electrodes and coherent tunneling contribution in epitaxial MTJs.
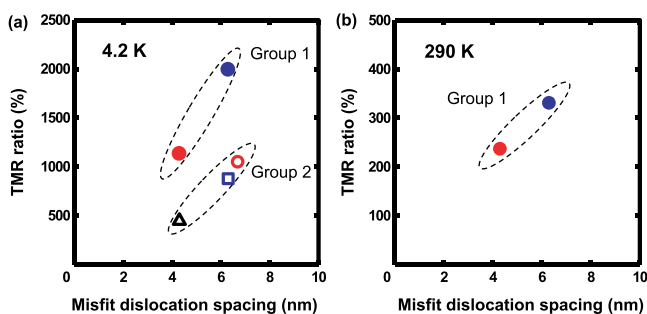

FIG. 4. Dependence of the TMR ratios at (a) 4.2 K and (b) 290 K on the average misfit dislocation spacing at the lower and upper interfaces with a MgO barrier for MTJs of group 1, including the CoFe-buffered Co_2MnSi/MgO/Co_2MnSi MTJ (blue solid circles) and MgO-buffered Co_2MnSi/MgO/Co_2MnSi MTJ (red solid circles). The TMR ratios and the misfit dislocation spacing for the latter are taken from Refs. 26 and 29, respectively. For comparison, similar dependences at 4.2 K for MTJs of group 2 (Ref. 30), including (from the lower side) MgO buffer/Co_2MnSi/MgO/CoFe MTJs (black open triangle), CoFe buffer/Co_2MnSi/MgO/CoFe MTJs (blue open square), and CoFe/MgO/Co_2MnSi MTJs (red open circle) having Mn-rich $Co_2Mn_{1.29}Si_{1.0}$, $Co_2Mn_{1.35}Si_{0.88}$, and $Co_2Mn_{1.29}Si_{1.0}$ electrodes, respectively, are also plotted in (a).

[1]S. A. Wolf, D. D. Awschalom, R. A. Buhrman, J. M. Daughton, S. von Molnár, M. L. Roukes, A. Y. Chtchelkanova, and D. M. Treger, Science **294**, 1488 (2001).

[2]I. Žutić, J. Fabian, and S. Das Sarmar, Rev. Mod. Phys. **76**, 323 (2004).

[3]R. A. de Groot, F. M. Mueller, P. G. van Engen, and K. H. J. Buschow, Phys. Rev. Lett. **50**, 2024 (1983).

[4]C. Felser, G. H. Fecher, and B. Balke, Angew. Chem., Int. Ed. **46**, 668 (2007).

[5]S. Kämmerer, A. Thomas, A. Hütten, and G. Reiss, Appl. Phys. Lett. **85**, 79 (2004).

[6]Y. Sakuraba, M. Hattori, M. Oogane, Y. Ando, H. Kato, A. Sakuma, T. Miyazaki, and H. Kubota, Appl. Phys. Lett. **88**, 192508 (2006).

[7]T. Ishikawa, T. Marukame, H. Kijima, K.-i. Matsuda, T. Uemura, M. Arita, and M. Yamamoto, Appl. Phys. Lett. **89**, 192505 (2006).

[8]M. Yamamoto, T. Marukame, T. Ishikawa, K.-i. Matsuda, T. Uemura, and M. Arita, J. Phys. D: Appl. Phys. **39**, 824 (2006).

[9]N. Tezuka, N. Ikeda, F. Mitsuhashi, and S. Sugimoto, Appl. Phys. Lett. **94**, 162504 (2009).

[10]W. Wang, E. Liu, M. Kodzuka, H. Sukegawa, M. Wojcik, E. Jedryka, G. H. Wu, K. Inomata, S. Mitani, and K. Hono, Phys. Rev. B **81**, 140402(R) (2010).

[11]T. Furubayashi, K. Kodama, H. Sukegawa, Y. K. Takahashi, K. Inomata, and K. Hono, Appl. Phys. Lett. **93**, 122507 (2008).

[12]Y. Sakuraba, K. Izumi, T. Iwase, S. Bosu, K. Saito, K. Takanashi, Y. Miura, K. Futatsukawa, K. Abe, and M. Shirai, Phys. Rev. B **82**, 094444 (2010).

[13]S. Picozzi, A. Continenza, and A. J. Freeman, Phys. Rev. B **69**, 094423 (2004).

[14]B. Hülsen, M. Scheffler, and P. Kratzer, Phys. Rev. B **79**, 094407 (2009).

[15]S. Ishida, S. Fujii, S. Kashiwagi, and S. Asano, J. Phys. Soc. Jpn **64**, 2152 (1995).

[16]S. Picozzi, A. Continenza, and A. J. Freeman, Phys. Rev. B **66**, 094421 (2002).

[17]I. Galanakis, P. H. Dederichs, and N. Papanikolaou, Phys. Rev. B **66**, 174429 (2002).

[18]P. J. Webster, J. Phys. Chem. Solids **32**, 1221 (1971).

[19]W. H. Butler, X.-G. Zhang, T. C. Schulthess, and J. M. MacLaren, Phys. Rev. B **63**, 054416 (2001).

[20]J. Mathon and A. Umerski, Phys. Rev. B **63**, 220403(R) (2001).

[21]S. Yuasa, T. Nagahama, A. Fukushima, Y. Suzuki, and K. Ando, Nature Mater. **3**, 868 (2004).

[22]S. S. Parkin, C. Kaiser, A. Panchula, P. M. Rice, B. Hughes, M. Samant, and S.-H. Yang, Nature Mater. **3**, 862 (2004).

[23]D. D. Djayaprawira, K. Tsunekawa, M. Nagai, H. Maehara, S. Yamagata, N. Watanabe, S. Yuasa, Y. Suzuki, and K. Ando, Appl. Phys. Lett. **86**, 092502 (2005).

[24]S. Ikeda, J. Hayakawa, Y. Ashizawa, Y. M. Lee, K. Miura, H. Hasegawa, M. Tsunoda, F. Matsukura, and H. Ohno, Appl. Phys. Lett. **93**, 082508 (2008).

[25]Y. Miura, H. Uchida, Y. Oba, K. Nagao, and M. Shirai, J. Phys.: Condens. Matter **19**, 365228 (2007).

[26]T. Ishikawa, H.-x. Liu, T. Taira, K.-i. Matsuda, T. Uemura, and M. Yamamoto, Appl. Phys. Lett. **95**, 232512 (2009).

[27]M. Yamamoto, T. Ishikawa, T. Taira, G.-f. Li, K.-i. Matsuda, and T. Uemura, J. Phys.: Condens. Matter **22**, 164212 (2010).

[28]F. Bonell, S. Audrieu, C. Tiusan, F. Montaigne, E. Snoeck, B. Belhadji, L. Calmels, F. Bertran, P. Le Fèvre, and A. Taleb-Ibrahimi, Phys. Rev. B **82**, 092405 (2010).

[29]T. M. Nakatani, Y. K. Takahashi, T. Ishikawa, M. Yamamoto, and K. Hono, J. Magn. Magn. Mater. **322**, 357 (2010).

[30]H.-x. Liu, Y. Honda, K.-i. Matsuda, M. Arita, T. Uemura, and M. Yamamoto, Jpn. J. Appl. Phys. **51**, 093004 (2012).